Journal of Materials Chemistry C

PAPER

View Article Online
View Journal | View Issue

Modeling of threshold and dynamics behavior of organic nanostructured lasers†

Cite this: J. Mater. Chem. C, 2014, 2, 1463

Song-Liang Chua,*[ab] Bo Zhen,[a] Jeongwon Lee,[a] Jorge Bravo-Abad,[c] Ofer Shapira[ad] and Marin Soljačić[a]

Organic dye molecules offer significant potential as gain media in the emerging field of optical amplification and lasing at subwavelength scales. Here, we investigate the laser dynamics in systems comprising subwavelength-structured cavities that incorporate organic dyes. To this end, we have developed a comprehensive theoretical framework able to accurately describe the interaction of organic molecules with any arbitrary photonic structure to produce single-mode lasing. The model provides explicit analytic expressions of the threshold and slope efficiency that characterize this class of lasers, and also the duration over which lasing action can be sustained before the dye photobleaches. Both the physical properties of the dyes and the optical properties of the cavities are considered. We also systematically studied the feasibility of achieving lasing action under continuous-wave excitation in optically pumped monolithic organic dye lasers. This study suggests routes to realize an organic laser that can potentially lase with a threshold of only a few W cm^{-2}. Our work puts forward a theoretical formalism that could enable the advancement of nanostructured organic-based light emitting and sensing devices.

Received 22nd September 2013
Accepted 26th November 2013

DOI: 10.1039/c3tc31870b

www.rsc.org/MaterialsC

1. Introduction

Organic dye lasers with high tunability in the visible wavelengths have attracted interest for many years due to their low-cost processing, flexible choice of substrates, and large emission cross-sections that can cover the spectral region from ultraviolet to the near infrared. Electrically pumped organic semiconductor lasers are desirable from a practical standpoint but their realization has remained elusive due to their high thresholds, low charge-carrier mobility in organic materials, and efficient exciton annihilation process in solid-state organic media.[1–5] A compromise to the above is the hybrid electrically pumped organic lasers.[6,7] These lasers are optically pumped by small electrically driven inorganic diode lasers and exhibit the benefits of a direct electrical pumping scheme (*i.e.* voltage/current controlled), thus reducing the size and the cost of the polymer laser system. While optically pumped organic lasers have been widely demonstrated,[8–11] lasing is only possible with high peak power excitation sources of short pulses; no continuous-wave (CW) operated organic lasers have been demonstrated without liquid dye circulation.

The motivation for this work is to explore the feasibility of achieving low-threshold lasing in an optically pumped CW monolithic organic laser, where the organic medium is stationary with respect to the pump beam and lasing action is sustained over a time scale longer than all decay lifetimes of the dye. To achieve this, one would need to (i) lower the thresholds of existing organic lasers to levels that are commensurate with most commercial applications (typically few W cm^{-2}),[12] (ii) minimize the photobleaching effects in the organic media, and (iii) ensure thermal management of the devices. In the following, we assume that thermal effects produced by localized heating of the dyes under excitation are minimized over the lasing duration (*e.g.* a few tens of milliseconds in a non-flowing dye laser[13]) through a careful design of the device.[14] We focus instead on optimizing the physical properties of the dyes and optical properties of the cavities to achieve (i) and (ii), assuming a photobleaching rate determined by the system chemical composition of the organic molecule, the host matrix, and packaging. To do so, it is critical to develop a complete theoretical understanding of the physical mechanisms underlying lasing action in organic lasers.

Here, we introduce a theoretical framework that extends previous studies on organic dyes[15,16] in order to account for the full multi-level rate equations, the photobleaching of dyes, and the modification that a complex electromagnetic environment introduces to the radiative decay rates of the dyes with respect to their free space values (the so-called Purcell effect[17,18]). The

[a]Research Laboratory of Electronics, Massachusetts Institute of Technology, 77 Massachusetts Avenue, Cambridge, MA 02139, USA

[b]DSO National Laboratories, 20 Science Park Drive, Singapore 118230, Singapore. E-mail: csonglia@dso.org.sg

[c]Departamento de Física Teórica de la Materia Condensada and Condensed Matter Physics Center (IFIMAC), Universidad Autónoma de Madrid, 28049 Madrid, Spain

[d]QD Vision Incorporation, 29 Hartwell Avenue, Lexington, MA 02421, USA

† Electronic supplementary information (ESI) available. See DOI: 10.1039/c3tc31870b

formalism provides explicit analytic expressions of the threshold and slope efficiency that characterize this class of lasers, as well as the duration over which lasing action can be sustained before the dye photobleaches. In particular, using a solution of Rhodamine 6G (R6G) dye molecules as the gain medium, our model suggests routes to attain a low-threshold organic laser that can potentially lase at a few W cm^{-2}. We expect our findings to open a path to the realization of cheap and compact organic light sources based on the hybrid electrical pumping scheme, which will in turn open up several potential applications in the visible spectrum. Our results are also of importance in the context of loss-compensation and lasing action in nanophotonics, plasmonics, and metamaterials, where solutions of R6G are often incorporated as the active medium in the system.[19,20]

The paper is organized as follows: Section 2 (and Appendix A) discusses the general theoretical model. Section 2.3 focuses on lasing action in organic lasers under pulse excitations, where results predicted by the theoretical model have been verified with measurements. Section 3 presents a detailed analysis of organic lasers under CW excitations. Finally, in Section 4, we summarize our results and provide a set of conclusions.

2. Theoretical framework

As a general energy-level model of an organic molecule, we consider the three lowest singlet and two lowest triplet states. Fig. 1(a) illustrates the energy level diagram and the different energy transfer mechanisms that form the basic structure of our model. Often, a four-level gain model of only the two lowest singlet states (S_0 and S_1) suffices in analyzing systems where the influences of the triplet states are minimized, either by pulsed excitations with widths much shorter than the intersystem crossing lifetimes[21] or by fast circulation of the dye solutions.[14,22] In this work, we considered the full energy-level model shown in Fig. 1(a) and (b) to identify the key parameters (from both molecular and optical standpoints) that can be optimized in order to simultaneously decrease the thresholds, increase the slope efficiencies, and reduce the photobleaching rates under CW pumping in monolithic organic lasers. We would like to point out that while the model described here represents fluorescing molecules dispersed in an amorphous environment, it can be simply modified to other configurations such as solid-state Alq_3:DCM (based on Förster energy transfer) and crystalline organic molecules by modifying the model of the energy levels. In this work, the model is applied to the case of optically pumped lasing systems consisting of R6G molecules dissolved in a solution under CW and pulsed excitations.

The various processes in the gain model are described *via* rate equations (see Appendix A) which are presented in a form that is convenient for numerical analysis, and yet allow for direct relations to experimental parameters. The most general description of an energy level model includes terms representing the optically induced transitions that are characterized by their absorption and emission cross-sections, as well as the radiative and non-radiative relaxations that are characterized by their lifetimes. Optically induced transitions of molecules to the upper states act as resonant absorbers of the excitation and emitted light, while those to the lower states result in the stimulated emission of light, producing lasing photons when the pump power is above the threshold. On the other hand, radiative relaxation of molecules to the ground singlet state leads to the spontaneous emission of light. The non-radiative processes considered are the internal conversions due to rotational and vibrational relaxations, the intersystem crossing of the molecules from the excited singlet state S_1 to the triplet state T_1, as well as their subsequent de-excitations back to the ground state S_0. Photobleaching is also included in our analysis and is modeled as a loss of molecules in the triplet state at a rate that is dependent on the excitation conditions[23–25] (*i.e.* pump power and the presence of oxygen).

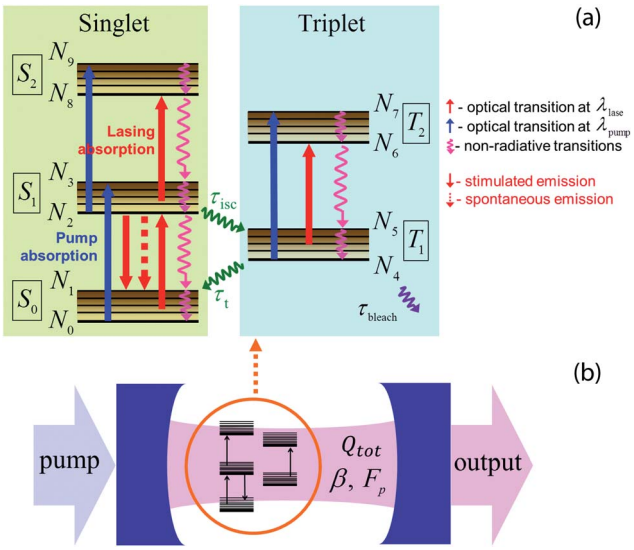

Fig. 1 Laser system consisting of an organic active medium embedded in a passive cavity. (a) The energy-level structure of the considered organic medium comprises of the three lowest singlet states of S_0, S_1, and S_2 and the two lowest triplet states of T_1 and T_2. Red (blue) solid vertical arrows are optically induced transitions at the lasing (excitation) wavelength whereas the dashed vertical arrow is the radiative decay of molecules (spontaneous emission). Wavy arrows are non-radiative transitions. Intersystem crossing of molecules from the singlet to triplet states is characterized by the decay lifetime τ_{isc} while the subsequent decay of triplets back to the ground singlet state is characterized by τ_t. Photobleaching in the organic medium is modeled as the loss of molecules from the triplet state at a rate of $1/\tau_{bleach}$ (represented as a violet wavy arrow). (b) Optical properties of the laser cavity are the spontaneous emission modification factor F_p, spontaneous emission coupling factor β, and the total quality factor Q_{tot} (see text for details of the definitions of these magnitudes).

Build-up of the triplet states' population can occur when T_1 is energetically closer to S_1 than S_0, resulting in the transition rate between S_1 and T_1 to be faster than that between T_1 and S_0. High occupancies in the triplet states have three detrimental effects on the lasing action: the population inversion becomes limited due to the smaller number of molecules in the singlet states, the fraction of the excitation light absorbed by the triplet states is increased, and dye absorption of the stimulated light is enhanced due to the overlapping emission and triplet-absorption spectrum. To overcome these effects, in organic

dye solutions for example, quenchers can be used to decrease the decay lifetime of the triplets.[26,27] Our model allows to study the effect of the intersystem crossing lifetime ratio (τ_t/τ_{isc}) on the triplet excited-state absorption.

The organic gain model is coupled to the semiclassical rate equation describing the population of the lasing photons. These photons are produced by stimulated and spontaneous emission, and at the same time, are resonantly reabsorbed by the organic media. In addition, the photons within the laser cavity are lost due to radiation into the far-field, intrinsic material absorption, and scattering from fabrication disorders in actual devices.

Using the organic laser model of Fig. 1 and the notations summarized in Table 1 of Appendix B, lasing action is obtained as follows: dye molecules are primarily excited from N_0 to N_3 at a rate proportional to the pump power P_{src}. The excited molecules then decay nonradiatively into N_2 after a lifetime τ_{32}. A net decay of molecules from N_2 to N_1 occurs through stimulated and spontaneous emission, as well as nonradiative relaxation. Some of the molecules in N_2, however, decay to the triplet state T_1 and are trapped if this decay occurs much faster than that of triplets back to the ground singlet states (*i.e.* $\tau_{isc} \ll \tau_t$). The resulting reduction in the number of molecules in the singlet states leads to a reduced population inversion, which implies a lower gain. Moreover, a high population of triplet states will also increase the lasing photon absorption and the number of molecules that are permanently lost through photobleaching. Molecules that make it to N_1 then decay nonradiatively to N_0 with a lifetime τ_{10}. If the pumping rate exceeds the net decay rate of molecules in N_2, then a population inversion between N_2 and N_1 can be easily achieved because N_2 depopulates slower compared to N_1 and N_3 (*i.e.* $\tau_{21} \gg \tau_{10} \approx \tau_{32}$). Lasing occurs beyond a threshold P_{src}^{thr} when the inversion leads to a gain that is sufficiently large to overcome the total losses in the dye and the cavity. Dye absorptions of the emitted lasing photons also occur in the singlet states where the molecules in S_0 and S_1 are optically excited to S_1 and S_2 respectively.

2.1. Subwavelength-structured cavity effects

We now turn to considering the subwavelength-structured cavity effects on the excited state emission lifetime of the molecules. The significant modification of the optical density of states in this class of structures with respect to the free-space case leads, in turn, to a substantial change of the corresponding spontaneous emission rate with respect to free-space emission. Specifically, within the Weisskopf–Wigner approximation, the spontaneous emission rate is proportional to the density of states.[28] We quantify this modification to the spontaneous emission rate centered near the lasing frequency f_l by including the factor F_p into the rate equations. We have defined $F_p = \gamma_{\text{all modes}}^{cav}/\gamma_{\text{all modes}}^{bulk}$, where $\gamma_{\text{all modes}}^{cav}$ is the total emission rate in the presence of a cavity and $\gamma_{\text{all modes}}^{bulk}$ ($= 1/\tau_{spont}$) is the total emission rate of the bulk media in free space (τ_{spont} is the corresponding spontaneous emission lifetime of the free-space medium). The inclusion of F_p in the model allows us to study the influence of the modified emission rate on the onset of lasing in novel nanostructured cavity designs.

Thus, the modified spontaneous emission rate in the presence of a cavity suitably designed for such a purpose can be expressed as[29,30]

$$\gamma_{f_l}^{cav} = \frac{\gamma_{f_l}^{cav}}{\gamma_{\text{all modes}}^{cav}} \times \frac{\gamma_{\text{all modes}}^{cav}}{\gamma_{\text{all modes}}^{bulk}} \times \gamma_{\text{all modes}}^{bulk} = \beta \times F_p \times \frac{1}{\tau_{spont}} \quad (1)$$

where β is the spontaneous emission coupling factor ($\beta \equiv \gamma_{f_l}^{cav}/\gamma_{\text{all modes}}^{cav}$) and $\gamma_{f_l}^{cav}$ is the emission rate into the lasing mode. In conventional, large cavities, where no enhancement of the spontaneous emission exists, $F_p = 1$.

2.2. Continuous-wave lasing system

In this section, we focus on the operation of the considered lasing system under CW excitation. In order to do that, we analytically solve the coupled rate equations of eqn (8) to (18) (Appendix A) in steady-state. The extension of these results to accommodate pulse excitations is presented in Section 2.3.

An analytical expression for the lasing threshold, which accounts for all relevant physical properties of the organic molecules and optical properties of the cavities, allows us to identify the relative importance of the various parameters in lowering the threshold under practical constraints. These constraints include the upper bound of a cavity's quality factor, the relative intersystem crossing lifetimes τ_t/τ_{isc} accessible to experiments, and the highest concentration of organic dye that one can use before its quantum yield reduces. Similarly, an analytical expression that predicts the photobleaching time of a dye will allow one to design systems that prolong the duration over which lasing action is possible. We separate the steady-state analysis into two parts: (i) predictions of the threshold and slope efficiency assuming no photobleaching and (ii) prediction of the time the dye takes to photobleach.

2.2.1. Threshold. The relatively slow photobleaching process can be ignored in the predictions of thresholds since τ_{bleach} is typically a few milliseconds (in air saturated solution at room temperature[24,31]) while the next longest lifetime is the triplet decay from T_1 to S_0 (*i.e.* τ_t), which varies between 10^{-7} and 10^{-4} seconds (in R6G depending if a solid-state or solution is used, or if a quencher is added). In other words, the effects of photobleaching only kick in after the lasing action begins. Under such assumption, the total molecular population is conserved in our model (*i.e.* $dN_{tot}/dt = 0$) so that the gain will become saturable at a high pump rate. We limit our analysis to the regime near the threshold where the effects of the gain medium on the field remain linear.[32] We also assume that the total molecular population $N_{tot} = N_{tot}^{den} \times V = N_0 + N_2 + N_4$ because molecules in the other levels are depleted due to their fast relaxation rates (this assumption breaks down only at very high excitation powers). N_{tot}^{den} is the density of dye molecules.

The steady state threshold power P_{src}^{thr} is then found by extrapolation of the linear input–output power curve to zero output, which yields:

$$\frac{\eta^{S_0S_1} P_{src}^{thr}}{hf_p} = \frac{V\left(F_p/\tau_{spont} + 1/\tau_{21} + 1/\tau_{isc}\right)/\tau'_{loss}}{F_p\beta V\Gamma_s/\tau_{spont} - (1+\tau_t/\tau_{isc})/N_{tot}^{den}\tau''_{loss}} \quad (2)$$

where $\eta^{S_0S_1}$ is the fraction of pump power absorbed by the S_0S_1 transition of the organic medium, h is the Planck's constant, and f_p is the excitation frequency. $1/\tau'_{loss} = 1/\tau_{loss} + v_g\sigma_{abs}^{S_0S_1}\Gamma_s N_{tot}^{den}$ and $1/\tau''_{loss} = 1/\tau_{loss} + v_g\sigma_{abs}^{T_1T_2}\Gamma_s N_{tot}^{den}$ are the total loss-rates of the lasing photons; the first and the second summands account for losses in the cavity and absorptions in the organic medium, respectively. τ'_{loss} accounts for the absorptions in the singlet states while τ''_{loss} accounts for those in the triplet states. τ_{loss} is the photon decay lifetime in the passive cavity and is related to its total quality factor by $Q_{tot} = 2\pi f_l\tau_{loss}$. It accounts for the losses due to radiation into the far-field, scattering from surface roughness and intrinsic material absorption in actual devices. v_g is the group velocity of the lasing mode and Γ_s is its fractional energy contained in the organic region. In deriving eqn (2), $\beta\Gamma_s$ is assumed to be much less than one and the relative magnitudes of the self-absorption cross-sections are assumed to follow that in Table 1 of Appendix B for R6G in solution. Since $\sigma_{abs}^{S_1S_2} \approx \sigma_{abs}^{T_1T_2}$, the total photon loss rates in both the S_1S_2 and T_1T_2 states may be represented by $1/\tau''_{loss}$ in our equations. We also note that the βV quantity is typically regarded to be volume-independent because β generally scales as the inverse of V in bulk systems.[33–35]

From the denominator of eqn (2), it becomes clear that lasing can only be realized in systems that satisfy

$$\frac{F_p\beta\Gamma_s N_{tot}}{\tau_{spont}} > \frac{(1+\tau_t/\tau_{isc})}{\tau''_{loss}}. \quad (3)$$

The above relationship implies that in laser systems where the intrinsic losses are higher than the maximal gain available, lasing cannot be attained regardless of the pump power. To overcome this, one should thrive to increase the concentration of the organic media (while taking care to maintain high quantum yield), increase the confinement and β factors through optimizing the cavity designs, and reduce the losses in both dyes and cavities.

In particular, nanostructured materials, such as distributed feedback structures and photonic crystals, can be engineered to support delocalized resonances with long decay lifetimes, leading to enhanced interactions of light with the organic molecules.[12,36] Moreover, these nanostructures may increase the β factors through modification of the spectral density of states,[37] where both the spectral and angular radiation of the molecules are altered (when compared to their free-space emission).[36] In view of eqn (3), it is also important to realize that in the case of multimode laser systems featuring broad gain linewidths (so that a large number of cavity modes lie within the gain curve), the Purcell enhancement is not expected to influence significantly the lasing threshold – essentially because in this case the Purcell increase on the magnitude of F_p is cancelled out by the corresponding decrease of the β factor.

2.2.2. Efficiency. The quantum slope efficiency of the laser is defined as the probability that a lasing photon will be emitted with the absorption of a single pumping photon. It is proportional to the linear slope of the input–ouput power relationship above the threshold. Within our theoretical formalism, the quantum slope efficiency q_{lase} is given by:

$$q_{lase} = \frac{\Delta P_{out}}{\Delta P_{src}}\frac{f_p}{f_l} = \frac{\eta^{S_0S_1}}{\tau_{cav}^{rad}\Gamma_s} \times \frac{F_p\beta V\Gamma_s/\tau_{spont} - (1+\tau_t/\tau_{isc})/N_{tot}^{den}\tau''_{loss}}{F_p\beta V/\tau_{spont}\tau_{loss} + v_g\sigma_{abs}^{S_0S_1}\left[1/\tau_{loss} + (1+\tau_t/\tau_{isc})/\tau''_{loss}\right]}. \quad (4)$$

τ_{cav}^{rad} is the photon decay lifetime of the cavity due to radiation into the far-field. The numerator in the second fraction of eqn (4) is equivalent to the denominator of the threshold expression in eqn (2), consistent with the fact that a low-threshold lasing system usually has high slope efficiency. In fact, if we replace the second fraction in eqn (4) with the total photon-loss lifetime of the laser system τ_{loss}^{tot}, a simple relationship for the slope efficiency can be found: $\Delta P_{out}/\Delta P_{src} \propto \eta^{S_0S_1}\tau_{loss^{tot}}/\tau_{rad^{cav}} \approx \eta^{S_0S_1}P_{rad^{cav}}/P_{loss^{tot}}$. In other words, the laser's slope efficiency depends on both the fraction of pump power that is absorbed by the organic medium and the fraction of the emitted power that is radiated into the far-field.

2.2.3. Photobleaching. Next, we include the photobleaching channel in N_4 through which a molecule becomes permanently lost and not return to the singlet states to further participate in the stimulated emission.[23] In this case, the total molecular population is no longer conserved but reduces according to $dN_{tot}/dt = -N_4/\tau_{bleach}$, where τ_{bleach} can be markedly different depending on the environment of the dyes (see Appendix A). This sets the time scale $\tau_{system}^{bleach} = \tau_{bleach}N_{tot}/N_4$ beyond which the dye photobleaches and the emitted signal is permanently quenched. In deriving eqn (5) below, the steady-state populations of N_4 and N_{tot} (assuming no photobleaching as in Sections 2.2.1 and 2.2.2) are substituted into the expression for τ_{system}^{bleach} above, even though N_4 and N_{tot} are now time-dependent quantities. We checked the validity of such an approximation by comparing the numerically predicted photobleaching rates using the full rate equations with the analytically predicted ones, and found their comparison to be good (illustrated in Section 3). As a passing remark, we point out that our model predicts τ_{system}^{bleach} to decrease linearly with the excitation power when operating below the lasing threshold. This linear trend of the bleaching rate with pump power is consistent with experimental observations.[13]

The photobleaching lifetime upon lasing (a volume-independent quantity) can be expressed as‡

$$\tau_{lase}^{bleach} = \tau_{bleach} \times F_{lase}^{bleach} \approx \tau_{bleach} \times \frac{N_{tot}^{den}\Gamma_s\tau'_{loss}}{\tau_t/\tau_{isc}}\left[\frac{F_p\beta V}{\tau_{spont}} - v_g\sigma_{abs}^{T_1T_2}\left(1+\frac{\tau_t}{\tau_{isc}}\right)\right] \quad (5)$$

Beyond this lifetime, the dye photobleaches and lasing shuts down. F_{lase}^{bleach} is the modification to τ_{bleach} afforded by the

‡ Note that $\tau_{lase}^{bleach} > 0$ so the systems considered can realize lasing [*i.e.* eqn (3) is satisfied].

specific design of the laser system; it depends on the dye concentration and intersystem crossing lifetime ratio (τ_t/τ_{isc}), as well as the cavity's quality factor, confinement factor, spontaneous emission coupling factor (β) and spontaneous emission modification factor (F_p). Again, the relative values of the absorption cross-sections in Table 1 are assumed in deriving eqn (5).

The quantum efficiency for dye bleaching, which gives the probability that a dye molecule will be bleached with the absorption of a single pumping photon, may similarly be derived as

$$q_{bleach} \approx \frac{N_{tot} h f_p}{\tau_{system}^{bleach} \eta^{S_0S_1} P_{src}}. \quad (6)$$

q_{bleach} is independent of the organic concentration. Its reciprocal $1/q_{bleach}$ provides an estimate of the number of times a molecule is recycled from S_0 to S_1 and back to S_0 before it is lost. Since $\tau_{system}^{bleach} \propto 1/P_{src}$ as noted above, q_{bleach} in eqn (6) is also independent of the excitation power (below the threshold).

2.3. Pulsed lasing system

Most lasing experiments involving organic gain materials are excited by short pulses,[8,9,38] except for systems where liquid dye circulation exist.[14,22] The key difference of the analysis in this section from that of the steady-state is that the undesirable triplet influences can now be minimized when the excitation pulse-width τ_{pulse} is shorter than the intersystem crossing lifetime τ_{isc}. This decoupling between the singlet and triplet states can be represented in our analytic model by setting τ_{isc} to large values so that $N_{tot}^{pulse} = N_0 + N_2$ at all times and no photobleaching takes place within the short lifespan of the lasing pulse signal. Physically, a large τ_{isc} value implies a quasi steady-state regime where the pulse length is assumed to be longer than all decay lifetimes of the molecules but remains shorter than τ_{isc}.

Moreover, the reabsorption of the lasing photons in S_1S_2 is sometimes neglected because the population of S_0 is much greater than that of S_1 so that $N_0\sigma_{abs}^{S_0S_1}$ is the dominant photon loss term in eqn (18) of Appendix A. As a result, a four-level gain model of the lower singlet states usually suffices in capturing the main lasing mechanisms. In this work, however, we include the photon absorption in S_1S_2 (since $\sigma_{abs}^{S_1S_2} \gg \sigma_{abs}^{S_0S_1}$ in some dyes such as R6G) and show that it plays a non-negligible role on the threshold values when $1/\tau_{loss}$ in $1/\tau_{loss}'$ becomes relatively small (*i.e.* $1/\tau_{loss}'' \approx v_g\sigma_{abs}^{S_1S_2}\Gamma_s N_{tot}/V$). Using the parameters of our lasing experiment,[36] this happens when $Q_{tot} = 2\pi f_l \tau_{loss} > 5 \times 10^5$ which is a physically realizable value.[39]

By setting τ_{isc} to infinity in eqn (2), the threshold pulse energy in the quasi steady-state regime is approximated as

$$U_{pulse}^{thr} = P_{src}^{thr}\tau_{pulse} \approx \frac{h f_p \tau_{pulse}}{\eta^{S_0S_1}} \times \frac{\left(F_p/\tau_{spont} + 1/\tau_{21}\right)/\tau_{loss}'}{F_p\beta V\Gamma_s/\tau_{spont} - 1/N_{tot}^{den}\tau_{loss}''} \times V. \quad (7)$$

In most pulsed lasing systems, τ_{pulse} and τ_{spont} are both on the order of a few nanoseconds and thus, the quasi steady-state approximation applied in eqn (7) leads to an underestimation of the threshold pulse energy. Nonetheless, eqn (7) is still useful in identifying the key molecular and photonic parameters needed to lower the lasing threshold. Similar to the steady-state regime of eqn (3), lasing can only take place when the maximal net gain is greater than the total cavity and molecular losses where $F_p\beta\Gamma_s N_{tot}/\tau_{spont} > 1/\tau_{loss}''$. However, unlike in eqn (3), these losses are no longer influenced by the triplet states.

2.3.1. Comparison with experiment. To verify our model, a pulsed lasing experiment with 1 mM R6G dissolved in methanol on top of a photonic crystal slab was conducted,[36] and its lasing threshold and slope are compared to numerical predictions. Fabrication and characterization of the passive photonic crystal cavity has been reported in a previous study by Lee *et al.*[40] The active cavity is optically excited near the peak of the dye's absorption spectrum at $\lambda_p = 532$ nm with 5 ns pulses at a repetition rate of 10 Hz. Lasing occurs at $\lambda_{lase} = 580$ nm where a strong optical resonance exists well within the R6G's emission spectrum, and having a confinement factor Γ_s of 7%. Q_{tot} is measured to be 8.3×10^3, Q_{cav}^{rad} is calculated to be 1.9×10^5, while β is approximated as 7×10^{-5} using the expression for bulk systems discussed in Appendix A. We input these parameters into our lasing model and observe that both the threshold and slope match well with the measured data, within experimental errors.[36] In particular, the measured threshold is 100 nJ while that predicted from our lasing model is 75 nJ.

3. Results and discussion

In this section, we analyze the steady-state operation of the R6G organic laser in terms of its threshold and the duration over which lasing action can be sustained before the dye photobleaches. The optical and physical properties of the system in eqn (2) and (5) are varied and their influences on the lasing performances are studied. The parameter values used in our examples are listed in Table 1 of Appendix B for R6G in solution. We begin the analysis by verifying the steady-state analytic expressions derived in Section 2. In particular, the analytic solutions are compared to the numerical solutions of the full model.

Fig. 2(a) illustrates the output intensity I_{out} (red curve) and photobleaching lifetime (blue curve) of the laser as a function of the excitation intensity I_{src}. The I_{out} value plotted corresponds to the quasi steady-state values before the laser emission is quenched [see Fig. 2(b)]. In this example, τ_t is assumed to be 10 μs so that $\tau_t/\tau_{isc} = 100$ and the threshold is found to be near 1 W cm^{-2}. By plotting the results against ηI_{src} in Fig. 2(a), we are able to account for the portion of incident power that is not absorbed by the dye; when $\eta < 1$, the threshold intensity would have to be scaled by $1/\eta$. For instance, if only 10% of the incident power is absorbed by the dye laser, then, the threshold becomes 10 W cm^{-2} instead. We also found that in this example, the quantum slope efficiency of the laser (calculated from the linear input–output intensity plot beyond threshold) is roughly 40% when $\eta = 1$. This matches the prediction of eqn (4) and is also consistent with the simple relationship of $q_{lase} = \Delta P_{out} f_p/\Delta P_{src} f_l \approx \eta P_{cav}^{rad}/P_{loss}^{tot}$ presented in Section 2. Specifically,

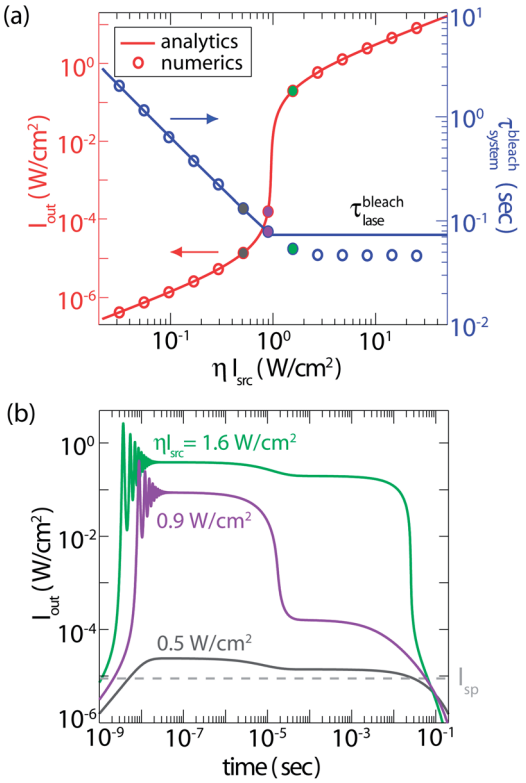

Fig. 2 (a) Output intensity I_{out} (red curve) and photobleaching lifetime (blue curve) of the organic laser as a function of the CW excitation intensity I_{src}. The plotted I_{out} values correspond to the quasi steady-state values before the laser emission is quenched [see the plot in (b)]. The circles are the results obtained from numerically solving the full set of rate equations in Appendix A while the solid lines are steady-state analytical solutions (outlined in Section 2.2) to the same rate equations. The filled circles correspond to the three excitation intensities analyzed in (b). η is the fraction of the pump power absorbed by the gain medium. (b) Temporal development of lasing action of the laser system in (a) for three ηI_{src} values near threshold. I_{sp} is the intensity level of spontaneous emission (see text for details of its definition).

$P^{rad}_{cav}/P^{tot}_{loss} = 50\%$ for the passive cavity considered in Table 1 and further reduction to 40% arises when the absorption losses in the dye's triplet states are included.

Next, we examine the photobleaching lifetime of the dye system under CW excitation. From Fig. 2(a), τ^{bleach}_{system} decreases linearly with the excitation intensity below threshold and clamps at its threshold value upon lasing. To understand this behavior, we first compute the bleaching quantum efficiency in eqn (6) and find $q_{bleach} = 5 \times 10^{-5}$. This implies that every molecule in the dye laser can be recycled to produce roughly $q_{lase}/q_{bleach} = 8 \times 10^3$ emitted photons before it is annihilated in N_4. When the pump rate is high, the molecules are recycled through the S_0S_1 states at a faster rate; each molecule reaches its maximum emission of 8×10^3 photons in a shorter time period. Hence, the photobleaching rate increases linearly with the excitation intensity. However, once the lasing is attained, the additional pumping power above threshold is channeled entirely into the coherently oscillating cavity mode and τ^{bleach}_{system} clamps at its threshold value of τ^{bleach}_{lase} [eqn (5)].

We note that q_{bleach} can be reduced by up to two orders of magnitude if an appropriate triplet quencher for R6G is used to reduce τ_t/τ_{isc} from 100 to 1. It can also be reduced by lengthening τ^{bleach} through chemically modifying the environment of the R6G molecules. For example, it is known that lowering water and oxygen results in a decreased photobleaching rate. Care should, however, be taken in this case to manage the parallel increase in triplet state population (oxygen is also a quencher of the triplet states)[25] to ensure a net reduction of q_{bleach}.

As seen in Fig. 2(a), the agreement between the analytical and numerical results are excellent, except for the τ^{bleach}_{lase} value which differs by a factor of ~1.5. The mismatch occurs because the analytical solutions consider the steady-state N_4 and N_{tot} values (without photobleaching) even though they are in fact time-dependent quantities (see Section 2). Nonetheless, this discrepancy remains smaller than a factor of 2 in all the examples considered and does not affect the conclusions drawn.

Fig. 2(b) shows the temporal development of lasing action in the same laser for three ηI_{src} values near threshold. Below threshold at $\eta I_{src} = 0.5$ W cm^{-2}, the output intensity is close to the spontaneous emission level I_{sp}. Within the semiclassical picture of spontaneous emission, this intensity corresponds to the energy of one photon[41] so that $I_{sp} = hf_l/\tau^{rad}_{cav}A_p$. A_p is the area under illumination. When ηI_{src} is increased to 0.9 W cm^{-2}, the laser is turned on initially between 10^{-8} s and 10^{-5} s where the output intensity reaches more than three orders of magnitude above I_{sp}. However, the laser shuts down at 10^{-5} s and the output decreases by two orders of magnitude to a quasi steady-state level before the dye photobleaches. The initial turn-on occurs when I_{src} is high enough to overcome the total losses in the singlet states. As the triplet states begin to populate, the associated absorption losses and trapping of molecules eventually quench the singlet inversion. At a higher pumping rate of $\eta I_{src} =$ 1.6 W cm^{-2}, the laser is turned on and the stimulated emission of light is sustained even after the triplet excited state absorption kicks in. In all the three cases above, dye emission ceased after 10^{-1} s due to photobleaching. Moreover, a series of very narrow spikes whose amplitudes die down with time can be observed upon turn on of the laser. These phenomena of spiking and relaxation oscillations are characteristics of laser systems in which the recovery time of the excited state population inversion is longer than the total decay time of the lasing mode.[41]

In Fig. 3 and 4, five parameters of the laser system are varied and their effects on the threshold (ηI^{thr}_{src}) and corresponding photobleaching modification factor (F^{bleach}_{lase}) are studied. These results are plotted using eqn (2) and (5) respectively. For illustration, the five parameters selected in this study are the total quality factor of the passive cavity (Q_{tot}), intersystem crossing lifetime ratio (τ_t/τ_{isc}), dye concentration, confinement factor (Γ_s), and the spontaneous emission modification factor (F_p). Practical values of Q_{tot} range from a few hundreds to tens of millions[39] and we expect the threshold intensity to decrease with increasing Q_{tot}. A reduced pumping intensity for lasing will in turn lengthen the time it takes for the dye to photobleach. In the following, we varied Q_{tot} with each of the other four parameters above to understand their effects on the laser characteristics.

3.1. Intersystem crossing lifetime ratio (τ_t/τ_{isc}) [Fig. 3(a) and 4(a)]

In eqn (2)–(5), the ratio τ_t/τ_{isc} plays an important role in influencing the lasing performances. A high τ_t/τ_{isc} value will not only increase the lasing threshold but also decrease the slope efficiency and lasing lifetime τ_{lase}^{bleach}. These observations can be understood from the accompanying build-up in the triplet state population, $N_4 = \tau_t/\tau_{isc} \times N_2$, through which high molecular- and photon-losses occur. Hence, it is desirable that the organic gain media have small values of τ_t/τ_{isc}. In R6G, triplet quenchers which affect τ_t are readily available and by simultaneously changing the environment of the molecules from solid to solution, τ_t/τ_{isc} can be varied over four orders of magnitudes from 1 to 10^4. The threshold plot illustrates a cut-off beyond which lasing shut down as τ_t/τ_{isc} increases. This happens when the triplet influence is so high that its associated photon absorption and molecular annihilation process overwhelmed the stimulated emission of light. In other words, eqn (3) cannot be satisfied. Note that high values of the lifetime ratio beyond 10^3 are typical in solid-state organic materials and based on our results, are major impediments to the attainment of low-threshold CW organic solid-state lasers. On the other hand, as τ_t/τ_{isc} decreases, the triplet states become less populated and the threshold values saturated towards that of a short-pulse system where only the energy transfers in the singlet states are relevant (see Section 2.3).

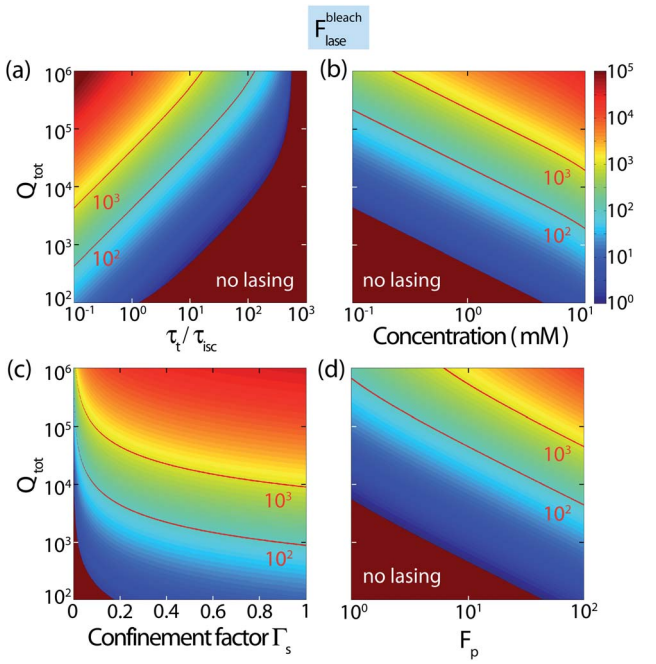

Fig. 4 Photobleaching modification factor (F_{lase}^{bleach}) as a function of the optical and physical properties in the same R6G organic laser system of Fig. 3.

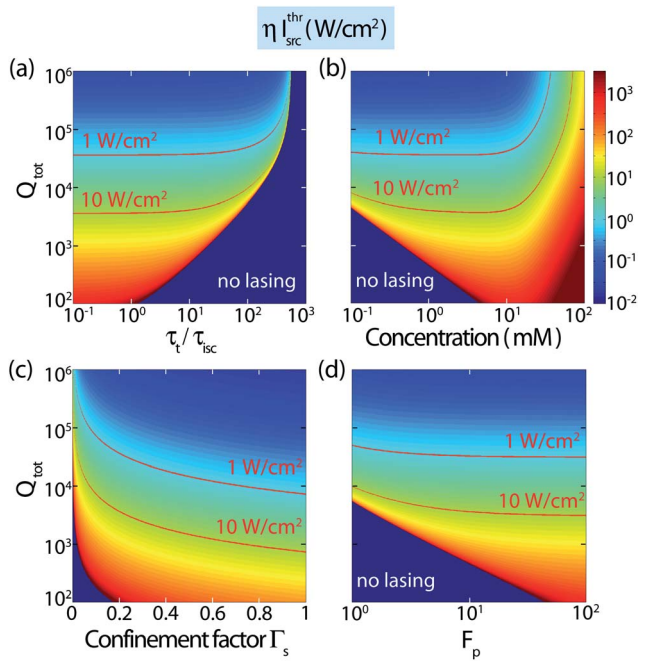

Fig. 3 Lasing threshold (ηI_{src}^{thr}) as a function of the optical and physical properties in a R6G organic laser under continuous excitation. η is the fraction of the excitation power absorbed by the dye. The parameter values used are listed in Table 1, except for the plot in (d) where τ_t is assumed to be 10 μs so that $\tau_t/\tau_{isc} = 100$ instead of 1. In particular, the total quality factor of the passive cavity (Q_{tot}) is varied with the intersystem crossing lifetime ratio (τ_t/τ_{isc}) in (a), the dye concentration in (b), the confinement factor (Γ_s) in (c), and the spontaneous emission modification factor (F_p) in (d).

Unlike the threshold values, the photobleaching factor in Fig. 4(a) does not saturate but continue to increase with declining τ_t/τ_{isc}. This trend is directly related to the corresponding reduced population of the N_4 state, where loss of the molecules takes place in our model. In our example, a threshold of $\eta I_{src}^{thr} = 0.7$ W cm^{-2} and photobleaching factor of $F_{lase}^{bleach} = 1125$ are predicted for the considered CW R6G organic laser when $Q_{tot} = 5 \times 10^4$ and $\tau_t/\tau_{isc} = 1$.

3.2. Dye concentration [Fig. 3(b) and 4(b)]

In diluted R6G with concentration below 5 mM, the quantum yield is high (*i.e.* $q_{dye} = 0.9$) and τ_{spont} is approximately 5 ns. As the concentration increases beyond 10 mM, both the quantum yield of the dye and its spontaneous emission lifetime begin to decrease.[42] We incorporate such concentration-dependent decrease in quantum yield and spontaneous emission lifetime into our model. From the threshold plot, we found that a minimum dye concentration is required for lasing to take place [*i.e.* eqn (3) is satisfied] when the cavity losses are high; dilute organic solutions cannot provide sufficient gain to overcome the total losses of the system. On the other hand, concentrated R6G solution above 10 mM is also undesirable because q_{dye} begins to decrease causing the threshold to rise rapidly. The decrease of q_{dye} is attributed to Förster-type excitation transfer from monomers to weakly fluorescing dimers, which are formed randomly at high concentrations.[42] Physically, a low q_{dye} implies that only a small fraction of the molecules excited into N_2 contributes to the emission of light. This leaves 5–10

mM to be the optimal concentration to operate the laser with the lowest threshold.

In Fig. 4(b), the photobleaching factor is observed to increase with concentration (up to 10 mM) for all values of Q_{tot}. This follows directly from the fact that a highly concentrated solution consists of more molecules (assuming the same volume of dye) able to participate in the excitation and de-excitation processes, and be recycled through the S_0S_1 states before they become quenched from photobleaching.

3.3. Confinement factor (Γ_s) [Fig. 3(c) and 4(c)]

A higher confinement factor leads to a larger modal gain in the system for the same excitation level, resulting in a reduction of the excitation threshold intensity.[43] This reduction in the threshold in turn increases the photobleaching factor, as observed in Fig. 4(c), and equivalently slows down the photobleaching rate. However, the decrease in both the threshold and photobleaching rate is dampened by the enhanced self-absorption of the dye at higher Γ_s, and hence, only a marginal improvement of the laser performances with increasing Γ_s is observed. The above description is applicable for $\Gamma_s > 0.1$ for the range of Q_{tot} considered. When $\Gamma_s < 0.1$, the laser performances deteriorate rapidly.

3.4. Spontaneous emission modification factor (F_p) [Fig. 3(d) and 4(d)]

In this example, τ_t is assumed to be 10 μs so that $\tau_t/\tau_{isc} = 100$ instead of 1 as considered in Table 1. F_p is the modification to the spontaneous emission rate of the free-space bulk organic dye ($1/\tau_{spont}$) in the presence of a cavity. It can be high in microcavities ($F_p = 75$) with small mode volumes, while maintaining its influence over a reasonably large spectrum of the emitter's bandwidth (quality factor of ~80).[44] From the threshold plot, we observed that F_p plays an important role in enabling lasing, especially at low Q_{tot}. However, its impact on threshold reduction diminishes as F_p increases; the F_p factors in the numerator and denominator of eqn (2) cancel out when the leading terms become dominating at large values of F_p. The physical interpretation is that a high F_p will not only lead to a desirable enhancement in the stimulated emission of light but also increase the spontaneous emission rate. Since the spontaneously emitted light is characterized as noise in a laser, the latter process is undesirable once lasing has taken place. In particular, spontaneous emission becomes a competing radiative process to stimulated emission through which molecules can decay radiatively out of the N_2 metastable state. When F_p becomes large, these two processes (stimulated and spontaneous emission) become equally dominant and the resulting reduction in threshold saturates.

On the other hand, the photobleaching lifetime of the dye does not saturate but continue to lengthen as F_p increases. This trend is directly related to the reduced population of the N_4 state when the total stimulated and spontaneous emission rates are enhanced.

In the analysis above, we have kept β unchanged to isolate the influence of F_p. We emphasize that, as mentioned in Section 2.2.1, in multimode cavities, when the gain linewidth is much broader than the cavity mode spacing, the reduction of the lasing threshold achieved by a larger value of F_p will be negated by the corresponding decrease of β.

4. Conclusions

We have presented a comprehensive theoretical analysis of lasing action in systems of subwavelength-structured cavities consisting of organic dye molecules. The formalism considers both the physical properties of the dyes and optical properties of the cavities, and provides explicit analytic expressions of the threshold and slope efficiency that characterize this class of lasers. Quenching of the laser emission due to photobleaching of the dyes is also considered. To illustrate this theoretical framework, we have analyzed in detail the case of lasing action from optically pumped monolithic R6G organic dye lasers. Our simulations have shown that for this system, with exemplary parameters listed in Table 1, a value for the threshold ηI_{src}^{thr} of a few W cm^{-2} can be achieved. Nanostructured materials that possess high quality factors and high spontaneous emission factors have been demonstrated[36,45] and are ideal resonators for realizing low-threshold organic lasers.[12] We believe that our results could contribute to enabling the advancement of nanostructured organic light emitting and sensing devices, as well as expanding the current understanding of gain-compensation and lasing action in plasmonic and metamaterial-based active devices.

A Appendix: rate equations

In this appendix, we first present the set of the spatially averaged coupled rate equations that are used to model the organic gain medium described by the processes shown in Fig. 1. As a general energy-level model of an organic molecule, we consider the three lowest singlet and two lowest triplet states. We then relate the optically induced transition terms of our model to the experimentally measured cross-sections σ, and show how such formalism can incorporate the influences of the cavity through the spontaneous emission modification factor F_p and spontaneous emission coupling factor β.

The rate equations of the molecular populations in each level (N_0 to N_9) and the semiclassical rate equation describing the lasing photon number ϕ_s can be written as

$$\frac{dN_0}{dt} = -\frac{P_{src}}{hf_p}\eta^{S_0S_1}\frac{(N_0 - N_3)}{N_{tot}} - v_g\sigma_{abs}^{S_0S_1}\Gamma_s\phi_s\frac{(N_0 - N_2)}{V} + \frac{N_1}{\tau_{10}} + F_p\frac{(1-\beta\Gamma_s)}{\tau_{spont}}N_2 \quad (8)$$

$$\frac{dN_1}{dt} = +F_p\frac{\beta}{\tau_{spont}}\Gamma_s\phi_s(N_2 - N_1) + N_2\left(F_p\frac{\beta\Gamma_s}{\tau_{spont}} + \frac{1}{\tau_{21}}\right) + \frac{N_4}{\tau_t} - \frac{N_1}{\tau_{10}} \quad (9)$$

$$\frac{dN_2}{dt} = -F_p\frac{\beta}{\tau_{spont}}\Gamma_s\phi_s(N_2-N_1) - v_g\sigma_{abs}^{S_1S_2}\Gamma_s\phi_s\frac{(N_2-N_8)}{V} - N_2\left(\frac{F_p}{\tau_{spont}}+\frac{1}{\tau_{21}}+\frac{1}{\tau_{isc}}\right) - \frac{P_{src}}{hf_p}\eta^{S_1S_2}\frac{(N_2-N_9)}{N_{tot}} + v_g\sigma_{abs}^{S_0S_1}\Gamma_s\phi_s\frac{(N_0-N_2)}{V} + \frac{N_3}{\tau_{32}} \quad (10)$$

$$\frac{dN_3}{dt} = +\frac{P_{src}}{hf_p}\eta^{S_0S_1}\frac{(N_0-N_3)}{N_{tot}} + \frac{N_8}{\tau_{83}} - \frac{N_3}{\tau_{32}} \quad (11)$$

$$\frac{dN_4}{dt} = -\frac{P_{src}}{hf_p}\eta^{T_1T_2}\frac{(N_4-N_7)}{N_{tot}} - v_g\sigma_{abs}^{T_1T_2}\Gamma_s\phi_s\frac{(N_4-N_6)}{V} + \frac{N_2}{\tau_{isc}} + \frac{N_5}{\tau_{54}} - \frac{N_4}{\tau_t} - \frac{N_4}{\tau_{bleach}} \quad (12)$$

$$\frac{dN_5}{dt} = +\frac{N_6}{\tau_{65}} - \frac{N_5}{\tau_{54}} \quad (13)$$

$$\frac{dN_6}{dt} = +v_g\sigma_{abs}^{T_1T_2}\Gamma_s\phi_s\frac{(N_4-N_6)}{V} + \frac{N_7}{\tau_{76}} - \frac{N_6}{\tau_{65}} \quad (14)$$

$$\frac{dN_7}{dt} = +\frac{P_{src}}{hf_p}\eta^{T_1T_2}\frac{(N_4-N_7)}{N_{tot}} - \frac{N_7}{\tau_{76}} \quad (15)$$

$$\frac{dN_8}{dt} = +v_g\sigma_{abs}^{S_1S_2}\Gamma_s\phi_s\frac{(N_2-N_8)}{V} + \frac{N_9}{\tau_{98}} - \frac{N_8}{\tau_{83}} \quad (16)$$

$$\frac{dN_9}{dt} = +\frac{P_{src}}{hf_p}\eta^{S_1S_2}\frac{(N_2-N_9)}{N_{tot}} - \frac{N_9}{\tau_{98}} \quad (17)$$

$$\frac{d\phi_s}{dt} = -\frac{v_g\Gamma_s\phi_s}{V}\left[\sigma_{abs}^{S_0S_1}(N_0-N_2) + \sigma_{abs}^{S_1S_2}(N_2-N_8) + \sigma_{abs}^{T_1T_2}(N_4-N_6)\right] - \frac{\phi_s}{\tau_{loss}} + F_p\frac{\beta}{\tau_{spont}}\Gamma_s\phi_s(N_2-N_1) + F_p\frac{\beta}{\tau_{spont}}\Gamma_sN_2. \quad (18)$$

It is implicitly implied in the above that P_{src}, N_i ($i = 0$ to 9), and ϕ_s are time-dependent quantities. $\eta^{S_0S_1}$, $\eta^{S_1S_2}$ and $\eta^{T_1T_2}$ are the fractions of pump power absorbed by the S_0S_1-, S_1S_2- and T_1T_2-transition of the organic dye, respectively. $N_{tot} = \sum_{i=0}^{9} N_i = N_{tot}^{den} \times V$ is the total molecular population obtained by taking the product of the molecular density and volume of the organic medium, and τ_{ij} is the non-radiative decay lifetime of the molecules from level i to j. In particular, τ_{21} is the non-radiative lifetime in N_2 and is related to the spontaneous emission lifetime by the dye's quantum yield q_{dye}, where $\tau_{21} = \tau_{spont} \times q_{dye}/(1 - q_{dye})$. Within our theoretical formalism, the laser output is computed as $P_{out} = hf_l\phi_s/\tau_{cav}^{rad}$, where τ_{cav}^{rad} is the photon decay lifetime of the passive cavity due to radiation into the far-field.

Excitation of molecules

In the excitation terms of the rate equations, P_{src} is the source power and $\eta^{S_0S_1}$ is the fraction of pump power absorbed by the S_0S_1 transition of the organic medium. The pump terms excite molecules from the S_0, S_1 and T_1 states to their respective higher energy levels separated by the photon energy hf_p. In a single-pass absorption of the pump light over a distance l, $\eta^{S_0S_1}$ is typically approximated by $\sigma_{pump}^{S_0S_1}\Gamma_p l N_{tot}^{den}$ where $\sigma_{pump}^{S_0S_1}$ is the experimentally measured absorption cross-section of the bulk medium at the excitation wavelength and Γ_p is the fractional energy of the pumping mode contained in the organic medium. However, in cases where the pump light is resonantly coupled into the organic medium and the absorption of light occurs over multiple passes, the relationship between η and σ_{pump} is less trivial. For instance, $\eta^{S_0S_1}$ is estimated by considering the total losses of the system (both absorption in the dye as well as radiation and scattering losses of the cavity) and applying the Q-matching arguments[46] when we compared the experimentally measured threshold and slope efficiency values to numerical predictions.[36]

Our numerical simulations of the full model considered pumping transitions in S_0S_1, S_1S_2 and T_1T_2 but only the excitation of the molecules from S_0 to S_1 is significant because its absorption cross-section is an order of magnitude larger than those in S_1S_2 and T_1T_2. Moreover, the population of the ground singlet state is also larger than those in S_1 and T_1, which further diminishes the importance of both S_1S_2 and T_1T_2 pumping transitions when operating at power levels near the lasing threshold. Thus, in deriving the analytic solutions in Section 2 of the main text, only the pumping transition from S_0 to S_1 is considered. Apart from the pump-induced excitations of the molecules, the emitted lasing light is also reabsorbed by the dye to excite molecules from the S_0, S_1 and T_1 states to their respective higher energy levels separated by the photon energy hf_l. These self-absorption transitions are represented in the rate equations using the cross-sections σ_{abs}.

Cavity effects

We now explain how the influences of the cavity are introduced into the stimulated and spontaneous emission terms of the rate equations. We begin by relating the experimentally measured stimulated emission cross-sections σ_{se} to the spontaneous emission coupling factor β. $\sigma_{se} = \lambda_l^4 g(\lambda_l)/8\pi c n_{eff}^2 \tau_{spont}$ in bulk organic media[42] and $\beta = \lambda_l^4 g(\lambda_l)/8\pi n_{eff}^3 V$ in bulk systems[33–35] (*i.e.* large resonators). In both relationships, $g(\lambda_l)$ is the photoluminescence spectrum normalized to the fluorescence quantum yield q_{dye},[42] n_{eff} is the effective index of the lasing mode, and c is the speed of light. From these expressions for σ_{se} and β for bulk systems, we find that $c\sigma_{se}/n_{eff}V = \beta/\tau_{spont}$. This relationship is used to replace the typical stimulated emission terms involving σ_{se} with $\beta\Gamma_s\phi_s$ $(N_2 - N_1)/\tau_{spont}$ in our rate equations. The term is directly proportional to the field intensity (through ϕ_s) as well as the population difference between the two levels connecting the transition (the energy separation between N_2 and N_1 is assumed to be hf_l). Such formulation of the stimulated emission term is consistent with those presented by Björk *et al.*[30] The cavity enhancement effects are then included in our model by replacing β/τ_{spont} with the modified spontaneous emission rate defined in eqn (1).

Intersystem crossing and triplet-state relaxation

In the rate equations, τ_{isc} is the intersystem-crossing lifetime of the molecules from S_1 to T_1, while τ_t is the triplet decay lifetime (both radiative and non-radiative) of molecules from T_1 to S_0. Phosphorescence arising from the decay of triplet molecules in T_1 is usually overshadowed by fluorescence in S_0S_1 (*i.e.* $\tau_{spont} \ll \tau_t$) and is not considered in our model. The transitions of molecules between the singlet and triplet states are energetically allowed but spin-forbidden, and so, they occur at a slower rate ($>10^{-7}$ s) than the singlet–singlet transitions ($<10^{-8}$ s). This allows the triplet influences in an organic laser system to be minimized by pumping with a pulse with width shorter than τ_{isc}, or by circulating the organic dye solution through the cavity at a rate faster than $1/\tau_{isc}$. It is critical to avoid a build up of the triplet population which tends to degrade the lasing performances by increasing the threshold and bleaching rate, while simultaneously decreasing the slope efficiency (see Section 2 of the main text).

Photobleaching

Photobleaching of the organic medium is modeled through the irreversible loss of molecules in the triplet state,[23] which is typically regarded as unstable due to its high chemical reactivity in an oxygen environment.[24,25] τ_{bleach} is the photobleaching lifetime in N_4. It can be markedly different depending whether the medium is exposed to an oxygen-rich or oxygen-deficient surrounding, or when different solvents are used with the dyes. It is sometimes also modeled to occur in the excited singlet state S_1.[25,31] In this work, we consider the conventional approach of modeling the loss of molecules in T_1 but note that the model can be extended to also include the photobleaching process in S_1.

B Appendix: parameter values

Table 1 provides the parameters used in the steady-state calculations of Section 3 based on solutions of R6G[42,47,48] (laser wavelength $\lambda_l = 580$ nm and pump wavelength $\lambda_p = 532$ nm):

Table 1 Parameters of the organic laser system based on R6G solution

Dye concentration	5 mM
Fluorescence quantum yield, q_{dye}	0.9
Spontaneous emission lifetime, τ_{spont}	5 ns
Intersystem crossing lifetime, τ_{isc}	100 ns
Triplet to singlet relaxation lifetime (quencher), τ_t	100 ns
Triplet photobleaching lifetime, τ_{bleach}	8 ms
Non-radiative relaxation lifetime from i to j, τ_{ij}	1 ps
Self-absorption cross-section in S_0S_1, $\sigma_{abs}^{S_0S_1}(\lambda_l)$	10^{-19} cm^2
Self-absorption cross-section in S_1S_2, $\sigma_{abs}^{S_1S_2}(\lambda_l)$	10^{-17} cm^2
Self-absorption cross-section in T_1T_2, $\sigma_{abs}^{T_1T_2}(\lambda_l)$	10^{-17} cm^2
Thickness of the gain region	30 nm
Confinement factor of the lasing mode, Γ_s	0.2
Spontaneous emission modification factor, F_p	1
Spontaneous emission coupling factor, β	1×10^{-4}
Total quality factor of passive cavity, Q_{tot}	5×10^4
Quality factor of cavity due to radiation-loss, Q_{cav}^{rad}	1×10^5

Acknowledgements

We acknowledge helpful discussions with Prof. Erich P. Ippen, Prof. John D. Joannopoulos and Prof. Steven G. Johnson. S.L.C. was supported in part by the MRSEC Program of the National Science Foundation under Award DMR-0819762. This work was also supported in part by the Army Research Office through the Institute for Soldier Nanotechnologies under Contract W911NF-13-D-0001. S.L.C. and M.S. were supported in part by the MIT S3TEC Energy Research Frontier Center of the Department of Energy under Grant DE-SC0001299. S.L.C. acknowledges the financial support from the DSO National Laboratories, Singapore. J.B.A. acknowledges financial support by the Ramon-y-Cajal program, Grant no. RyC-2009-05489.

References

1 T. Rabe, K. Gerlach, T. Riedl, H.-H. Johannes, W. Kowalsky, J. Niederhofer, W. Gries, J. Wang, T. Weimann, P. Hinze, F. Galbrecht and U. Scherf, *Appl. Phys. Lett.*, 2006, **89**, 081115.
2 R. Bornemann, U. Lemmer and E. Thiel, *Opt. Lett.*, 2006, **31**, 1669–1671.
3 Y. Zhang and S. R. Forrest, *Phys. Rev. B: Condens. Matter Mater. Phys.*, 2011, **84**, 241301.
4 N. C. Giebink and S. R. Forrest, *Phys. Rev. B: Condens. Matter Mater. Phys.*, 2009, **79**, 073302.
5 I. D. W. Samuel and G. A. Turnbull, *Chem. Rev.*, 2007, **107**, 1272–1295.
6 A. E. Vasdekis, G. Tsiminis, J.-C. Ribierre, L. O. Faolain, T. F. Krauss, G. A. Turnbull and I. D. W. Samuel, *Opt. Express*, 2006, **14**, 9211–9216.
7 J. Clark and G. Lanzani, *Nat. Photonics*, 2010, **4**, 438–446.
8 M. Koschorreck, R. Gehlhaar, V. G. Lyssenko, M. Swoboda, M. Hoffmann and K. Leo, *Appl. Phys. Lett.*, 2005, **87**, 181108.
9 V. G. Kozlov, V. Bulović, P. E. Burrows and S. R. Forrest, *Nature*, 1997, **389**, 362–364.
10 S. Chénais and S. Forget, *Polymer Int.*, 2012, **61**, 390–406.
11 S. Kena-Cohen and S. R. Forrest, *Nat. Photonics*, 2010, **4**, 371–375.
12 C. Karnutsch, C. Pflumm, G. Heliotis, J. C. deMello, D. D. C. Bradley, J. Wang, T. Weimann, V. Haug, C. Gärtner and U. Lemmer, *Appl. Phys. Lett.*, 2007, **90**, 131104.
13 E. P. Ippen, C. V. Shank and A. Dienes, *IEEE J. Quantum Electron.*, 1971, **7**, 178–179.
14 O. G. Peterson, S. A. Tuccio and B. B. Snavely, *Appl. Phys. Lett.*, 1970, **17**, 245–247.
15 O. G. Peterson, J. P. Webb, W. C. McColgin and J. H. Eberly, *J. Appl. Phys.*, 1971, **42**, 1917–1928.
16 R. A. Keller, *IEEE J. Quantum Electron.*, 1970, **6**, 411–416.
17 E. Purcell, *Phys. Rev.*, 1946, **69**, 681.
18 D. Kleppner, *Phys. Rev. Lett.*, 1981, **47**, 233–236.
19 P. Berini and I. De Leon, *Nat. Photonics*, 2012, **6**, 16–24.
20 O. Hess, J. B. Pendry, S. A. Maier, R. F. Oulton, J. M. Hamm and K. L. Tsakmakidis, *Nat. Mater.*, 2012, **11**, 573–584.
21 P. P. Sorokin, J. R. Lankard, V. L. Moruzzi and E. C. Hammond, *J. Chem. Phys.*, 1968, **48**, 4726–4741.

22 F. P. Shäfer, *Dye Lasers*, Springer, New York, 1990.
23 E. C. L. Ru and P. G. Etchegoin, *Principles of Surface-Enhanced Raman Spectroscopy: and related plasmonic effects*, Elsevier, Oxford, UK, 2009.
24 J. Widengren, U. Mets and R. Rigler, *J. Phys. Chem.*, 1995, **99**, 13368–13379.
25 J. Widengren and R. Rigler, *Bioimaging*, 1996, **4**, 149–157.
26 B. B. Snavely and F. P. Shäfer, *Phys. Lett.*, 1969, **28A**, 728–729.
27 R. Pappalardo, H. Samelson and A. Lempicki, *Appl. Phys. Lett.*, 1970, **16**, 267–269.
28 L. Novotny and B. Hecht, *Principles of Nano-Optics*, Cambridge Univ. Press, Cambridge, UK, 2006.
29 D. Englund, D. Fattal, E. Waks, G. Solomon, B. Zhang, T. Nakaoka, Y. Arakawa, Y. Yamamoto and J. Vučković, *Phys. Rev. Lett.*, 2005, **95**, 013904.
30 G. Björk and Y. Yamamoto, *IEEE J. Quantum Electron.*, 1991, **27**, 2386–2396.
31 C. Eggeling, J. Widengren, R. Rigler and C. A. M. Seidel, *Anal. Chem.*, 1998, **70**, 2651–2659.
32 S.-L. Chua, Y. D. Chong, A. D. Stone, M. Soljačić and J. Bravo-Abad, *Opt. Express*, 2011, **19**, 1539–1562.
33 A. Yariv and P. Yeh, *Photonics: Optical Electronics in Modern Communications*, Oxford University Press, New York, 2007.
34 K. Petermann, *IEEE J. Quantum Electron.*, 1979, **15**, 566–570.
35 T. Baba, T. Hamano, F. Koyama and K. Iga, *IEEE J. Quantum Electron.*, 1991, **27**, 1347–1358.
36 B. Zhen, S.-L. Chua, J. Lee, A. W. Rodriguez, X. Liang, S. G. Johnson, J. D. Joannopoulos, M. Soljačić and O. Shapira, *Proc. Natl. Acad. Sci. U. S. A.*, 2013, **110**, 13711–13716.
37 R. C. McPhedran, L. C. Botten, J. McOrist, A. A. Asatryan, C. M. de Sterke and N. A. Nicorovici, *Phys. Rev. E: Stat., Nonlinear, Soft Matter Phys.*, 2004, **69**, 016609.
38 V. Bulović, V. G. Kozlov, V. B. Khalfin and S. R. Forrest, *Science*, 1998, **279**, 553–555.
39 D. K. Armani, T. J. Kippenberg, S. M. Spillane and K. J. Vahala, *Nature*, 2003, **421**, 925–928.
40 J. Lee, B. Zhen, S.-L. Chua, W. Qiu, J. D. Joannopoulos, M. Soljačić and O. Shapira, *Phys. Rev. Lett.*, 2012, **109**, 067401.
41 A. E. Siegman, *Lasers*, Univ. Science Books, Mill Valley, California, 1986.
42 A. Penzkofer and W. Leupacher, *J. Lumin.*, 1987, **37**, 61–72.
43 L. A. Coldren, S. W. Corzine and M. L. Mašanović, *Diode Lasers and Photonic Intergrated Circuits*, John Wiley & Sons, Inc., Hoboken, New Jersey, 2012.
44 L. Sanchis, M. J. Cryan, J. Pozo, I. J. Craddock and J. G. Rarity, *Phys. Rev. B: Condens. Matter Mater. Phys.*, 2007, **76**, 045118.
45 H. Y. Ryu, M. Notomi, E. Kuramoti and T. Segawa, *Appl. Phys. Lett.*, 2004, **84**, 1067–1069.
46 D. L. C. Chan, I. Celanovic, J. D. Joannopoulos and M. Soljačić, *Phys. Rev. A*, 2006, **74**, 064901.
47 F. J. Duarte and L. W. Hillman, *Dye Laser Principles, with Applications*, Academic Press, Boston, MA, 1990.
48 L. Zhenyu and D. Psaltis, *Microfluid. Nanofluid.*, 2008, **4**, 145–158.